Supporting Information for

Diisopropylammonium Bromide Based Two-Dimensional Ferroelectric Monolayer Molecular Crystal with Large In-Plane Spontaneous Polarization

Liang Ma[†,§], Yinglu Jia[†], Stephen Ducharme[‡], Jinlan Wang[§] and Xiao Cheng Zeng*[,†,‡,‖]

[†]Department of Chemistry, University of Nebraska–Lincoln, Lincoln, NE 68588, United States
[§]School of Physics, Southeast University, Nanjing 211189, China
[‡]Department of Physics and Astronomy, Nebraska Center for Materials and Nanoscience, University of Nebraska-Lincoln, Lincoln, Nebraska 68588, United States
[‖]Department of Mechanical & Materials Engineering, University of Nebraska–Lincoln, Lincoln, Nebraska 68588, United States

*Email: xzeng1@unl.edu

I. Computational Details

Density functional theory (DFT) computations were performed by employing the projected augmented wave (PAW) potentials[1] and the exchange-correlation functional based on the Perdew-Burke-Ernzerhof (PBE)[2] functional within the generalized gradient approximation (GGA), all implemented in the Vienna ab initio simulation package (VASP 5.4).[3] The periodic replica of 2D DIPAB monolayer molecular crystal along *z* direction were separated by a vacuum space of > 15 Å to avoid potential artificial interaction among periodic images. For the optimization of lattice and atomic position, a 6 × 6 × 1 and 6 × 6 × 6 Monkhorst-Pack k-point meshes were used for the Brillouin zone integration sampling of 2D monolayer and for the 3D bulk of diisopropylammonium bromide (DIPAB), diisopropylammonium chloride (DIPAC) and diisopropylammonium iodide (DIPAI) molecular crystals, respectively. A denser 9 × 9 × 1 and 9 × 9 × 9 meshes were used for the calculation of electronic polarization of 2D and 3D systems, respectively.[4] The initial structures of DIPAB and DIPAC were taken from the experimental reports.[5] All structures were relaxed until the residual force component acting on each atom was less than 0.01 eV/Å. The convergence criteria for electronic relaxation was 10^{-5} eV. The energy cutoff for the plane-wave basis sets was set to be 400 eV. After careful comparison, we found that the optimized lattice parameters of bulk DIPAB crystal by using the PBE + vdW-D3 scheme[6] are comparable to or even better than those by using the meta-GGA type SCAN functional[7] + rVV10[8] vdW density functional scheme,[9] as the results are in good agreement ($\leq$ 3%) with the experimental results (Table S1). Due to much more computationally expensive SCAN + rVV10 method, here, only the PBE+D3 scheme was adopted for all computations.

It is known that the Berry-phase method can introduce the polarization indetermination quantum (PIQ) through multi-modulo of neR/V due to the periodic boundary condition– where e is the electron charge, R is a translation vector of the real-space lattice, V is the unit-cell volume and n is an integer. To obtain well-defined polarization, the PIQ (the n) has to be determined. In the present work, we determine the PIQ in the Berry-phase calculation of DIPAB molecular crystal by simply applying a point charge model for such an ionic system to roughly estimate the polarization. We carefully choose the unit cell of bulk DIPAB crystal so that the dipole moments will not be broken up by the cell boundaries (based on the experimental structure[5a]). The negative charge centers are assumed at the Br^- ions while the positive charge centers are assumed at the

geometric center of two H atoms of the $–[NH2]^+$ groups. We can estimate the polarization by using the equation of $P = \Sigma\ q*r$, where q is the charge (e for the $–[NH2]^+$ group and –e for the $Br^–$ ion) and r is the position vector of each charge center. The point charge model gives us an estimated polarization P_s of 20.77 μC $cm^{–2}$ for the bulk DIPAB molecular crystal. This benchmark test value can help to determine the PIQ number n in the Berry-phase calculation. The Berry-phase method finally gives a value of P_s of 22.1 μC $cm^{–2}$, which is in good agreement with the experimental value of 23 μC $cm^{–2}$.[5a] It is worth noting that the point charge model can give a reasonable estimation of P_s for the DIPAB molecular crystal. The difference in the computed P_s between point charge model and the Berry phase method can be attributed to the over-localized point charge model and neglected electron density distribution. Such a point charge model is also used to determine the PIQ number n in 2D monolayer DIPAB molecular crystal.

Table S1.Calculated lattice parameters of bulk DIPAB, DIPAC and DIPAI crystals, based on the PBE + D3 and SCAN + rVV10 schemes, and the corresponding experimental (Exp.) values.

Lattice	a (Å)	b (Å)	c (Å)	α (º)	β (º)	γ (º)
			DIPAB			
PBE+D3	7.55	7.79	7.62	90.00	116.54	90.00
SCAN+rVV10	7.49	7.75	7.56	90.00	116.65	90.00
Exp.[7]	7.766	8.034	7.836	90.000	116.346	90.000
			DIPAC			
PBE+D3	7.31	7.62	7.50	90.00	115.34	90.00
Exp.[8]	7.674	7.945	7.766	90.000	114.950	90.000
			DIPAI			
PBE+D3	7.74	7.93	7.78	90.000	117.13	90.00

II. Details for *Ab Initio* Molecular Dynamics Simulations.

Ab initio molecular dynamics (AIMD) simulations of 2D DIPAB monolayer molecular crystal were performed in the constant temperature (300 K) and pressure (0 GPa) (*NPT*) ensemble with the GGA-PBE functional and the D3 dispersion correction scheme, as implemented in the VASP 5.4. Both the atomic and lattice degrees of freedom were allowed to relax in the AIMD simulations, in which the Langevin thermostat[10] and the Parrinello-Rahman dynamics[11] were adopted. A 3×3 supercell (432 atoms) of 2D DIPAB (001) or (100) monolayer was placed on a $5\sqrt{3} \times 9$ rectangle graphene substrate (180 atoms) to ensure the lattice mismatch less than 5%. The graphene substrate was fixed in our AIMD simulation. To achieve the thermal equilibrium, a 5 ps AIMD simulation with time step of 1fs was performed for each system.

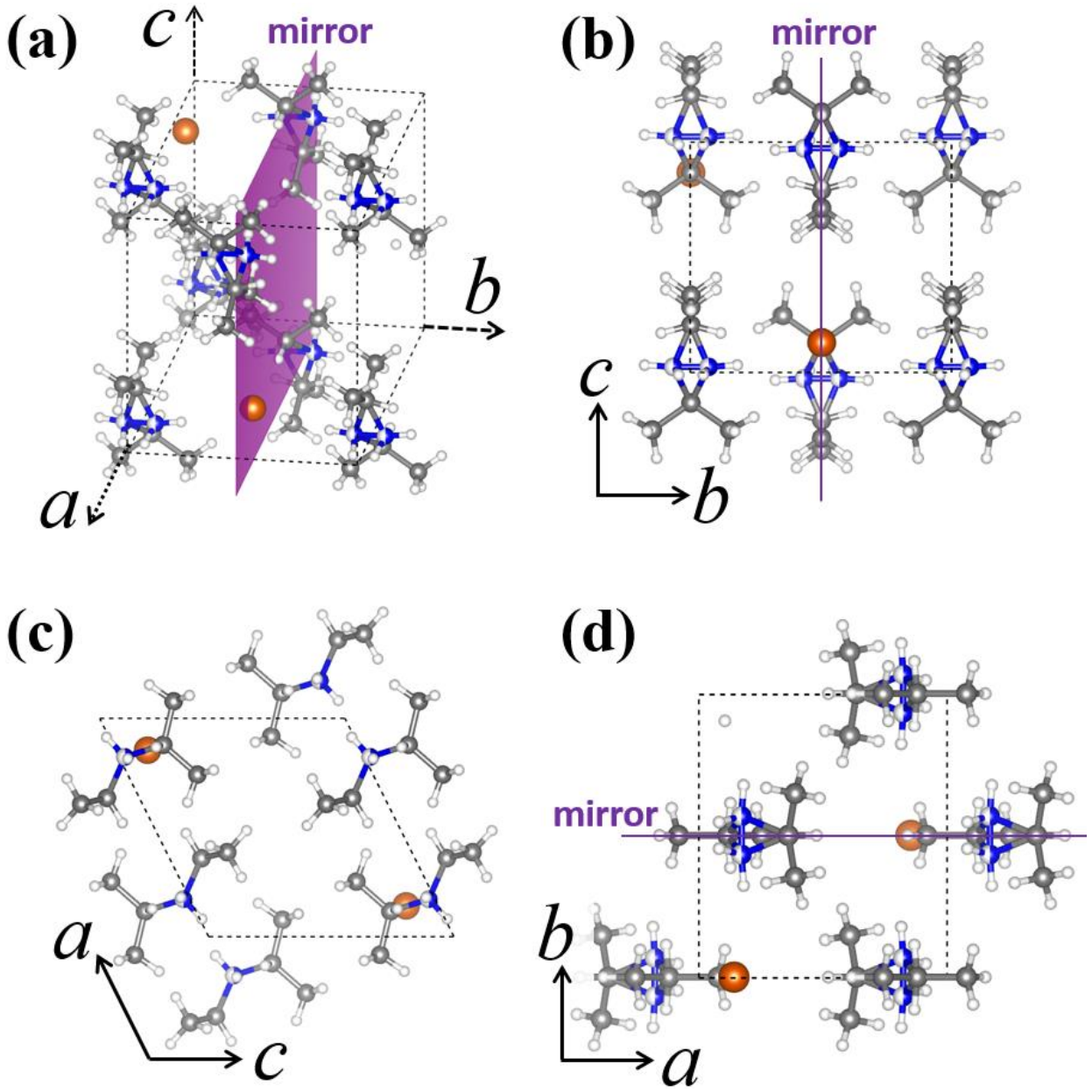

Figure S1. (a) Optimized structure of paraelectric bulk DIPAB crystal. The purple plane denotes the mirror plane of the paraelectric phase with space group $P2_1/m$. (b), (c) and (d) show the atomic views of paraelectric phase of DIPAB along *a*, *b* and *c* axis, respectively. The white, grey, blue and orange balls represent the H, C, N and Br atoms, respectively.

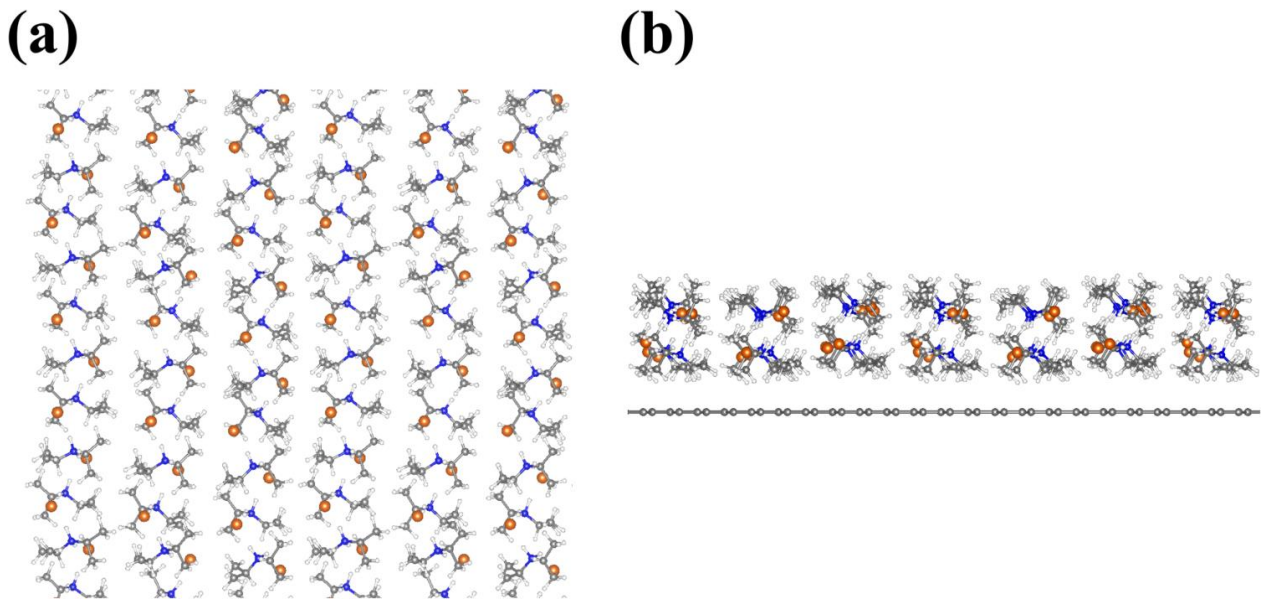

Figure S2. (a) Top and (b) side views of snapshots of the 2D DIPAB (100) monolayer after 5 ps of AIMD simulation (time step: 1 fs) in the *NPT* ensemble, where the temperature is controlled at 300 K and pressure is controlled at 0 GPa. Note that the substrate in top view is removed for clarity.

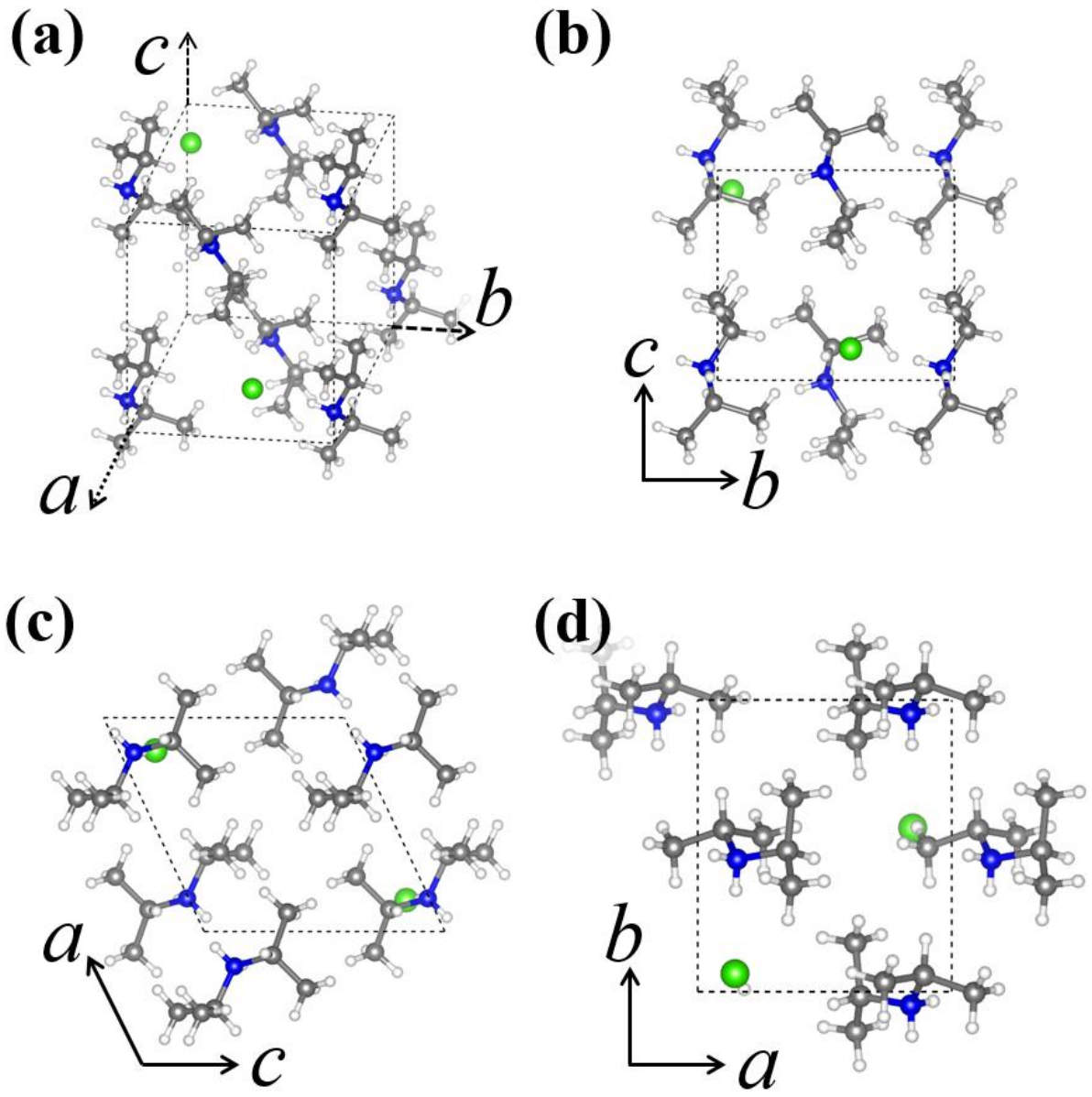

Figure S3. (a) Optimized structure of ferroelectric bulk DIPAC crystal. (b), (c) and (d) show the atomic views of ferroelectric phase of DIPAC along *a*, *b* and *c* axis, respectively. The white, grey, blue and green balls represent the H, C, N and Cl atoms, respectively.

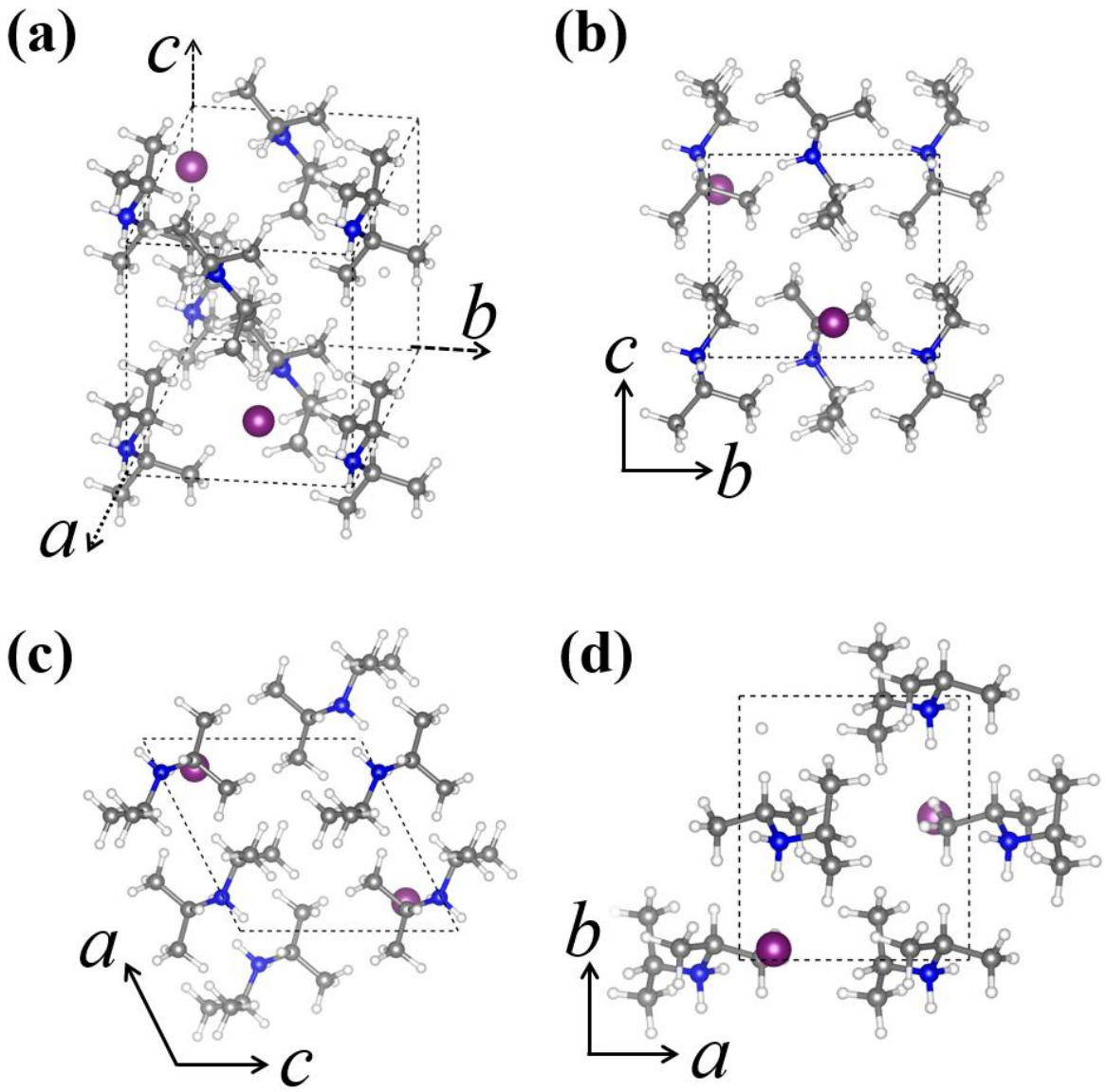

Figure S4. (a) Optimized structure of ferroelectric bulk DIPAI crystal. (b), (c) and (d) show the atomic views of the ferroelectric phase of DIPAI along *a*, *b* and *c* axis, respectively. The white, grey, blue and purple balls represent the H, C, N and I atoms, respectively.

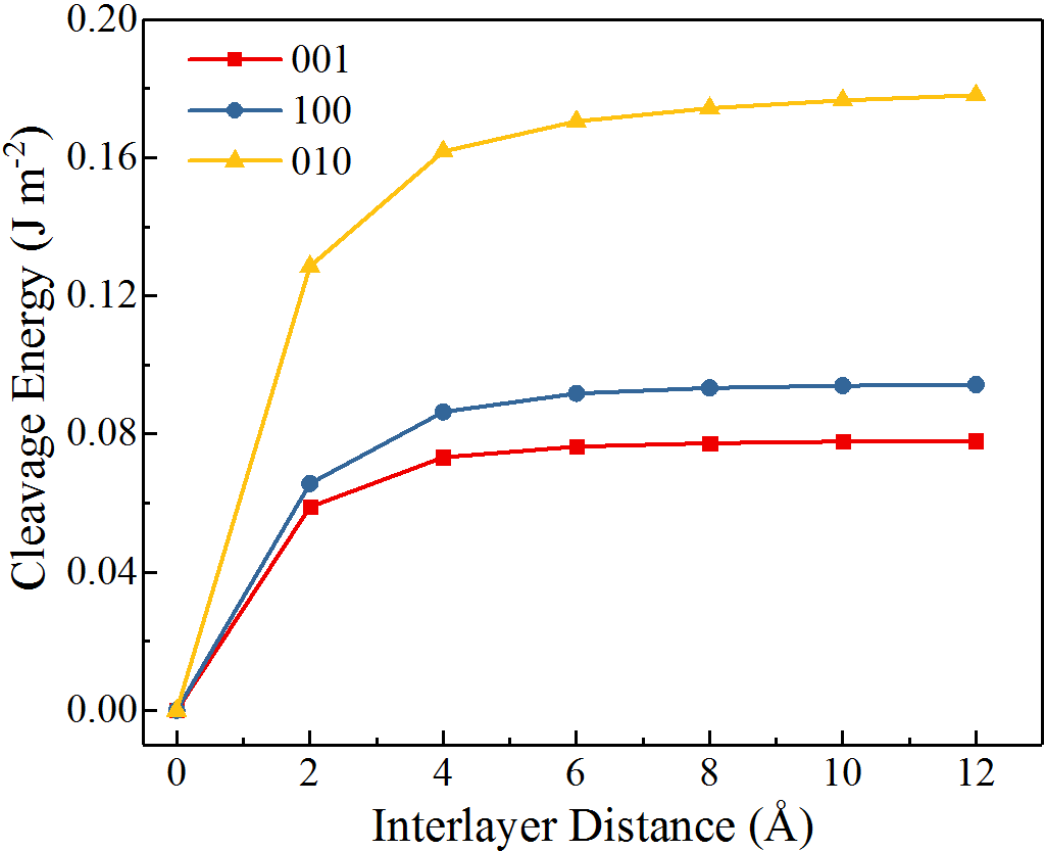

Figure S5. Cleavage energy estimation on the mechanical peeling of DIPAC along the (001), (100) and (010) planes, respectively, versus the interlayer distance. The reference starting point (0 Å) corresponds to the perfect ferroelectric bulk DIPAC crystal.

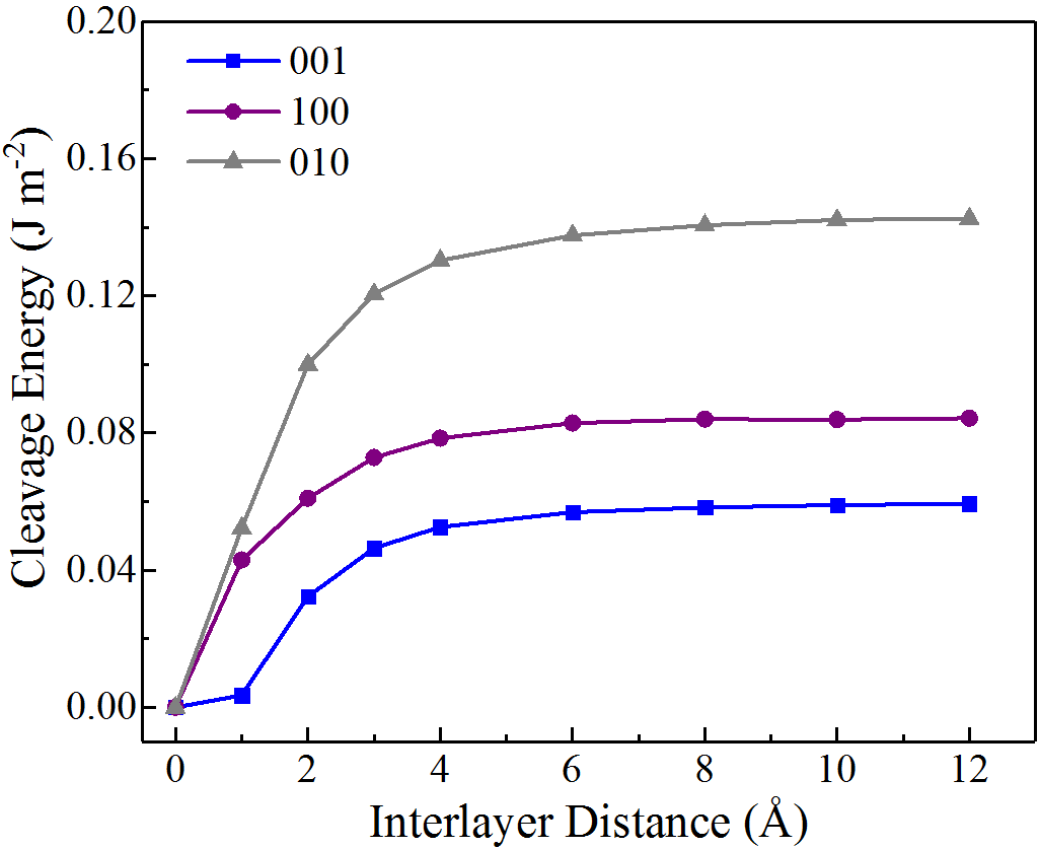

Figure S6. Cleavage energy estimation on the mechanical peeling of DIPAI along the (001), (100) and (010) plane, respectively, by increasing the interlayer distances. The reference starting point (0 Å) corresponds to the perfect ferroelectric bulk DIPAI crystal.

Table S2. Calculated lattice parameters and spontaneous polarization (P_s) of 2D DIPAC (001) and (100) monolayers, respectively.

	monolayer	a (Å)	b (Å)	γ (°)	P_s (10^{-6} μC cm^{-1})
DIPAC	(001)	7.23	7.58	90.00	1.61
	(100)	7.24	7.33	90.00	1.54
DIPAI	(001)	7.58	7.75	90.00	1.47
	(100)	7.16	7.63	90.00	1.61

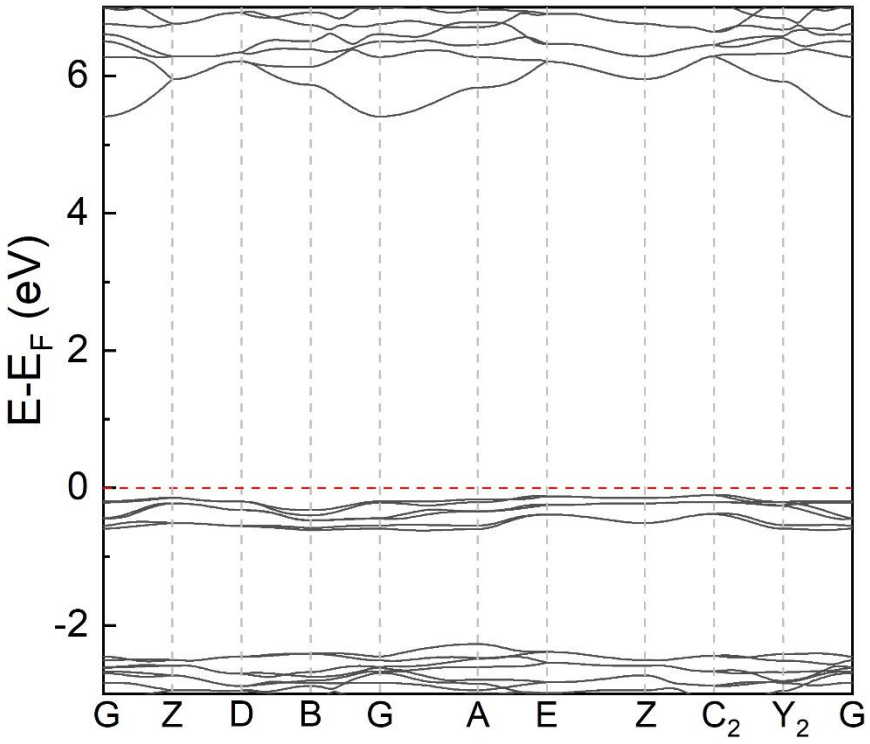

Figure S7. Computed electronic structure of 3D bulk DIPAB molecular crystal. The Fermi level is set to be zero (red dash line).

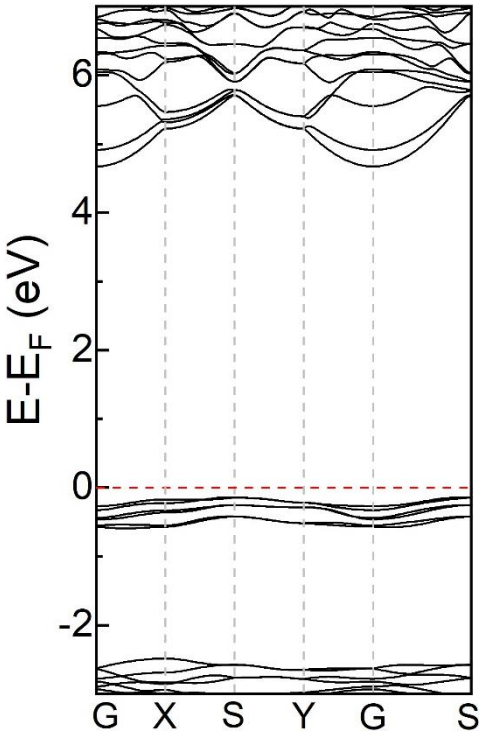

Figure S8. Computed electronic structure of 2D (001) monolayer DIPAB molecular crystal. The Fermi level is set to be zero (red dash line).

SUPPORTING REFERENCES

(1) (a) Blöchl, P. E. Projector Augmented-Wave Method. *Phys. Rev. B* **1994**, *50*, 17953-17979; (b) Kresse, G.; Joubert, D. From Ultrasoft Pseudopotentials to the Projector Augmented-Wave Method. *Phys. Rev. B* **1999**, *59*, 1758-1775.

(2) Perdew, J. P.; Burke, K.; Ernzerhof, M. Generalized Gradient Approximation Made Simple. *Phys. Rev. Lett.* **1996**, *77*, 3865-3868.

(3) (a) Kresse, G.; Furthmüller, J. Efficient Iterative Schemes for *Ab Initio* Total-Energy Calculations Using a Plane-Wave Basis Set. *Phys. Rev. B* **1996**, *54*, 11169-11186; (b) Kresse, G.; Furthmuller, J. Efficiency of Ab-Initio Total Energy Calculations for Metals and Semiconductors Using a Plane-Wave Basis Set. *Comput. Mater. Sci.* **1996**, *6*, 15-50.

(4) Monkhorst, H. J.; Pack, J. D. Special Points for Brillouin-Zone Integrations. *Phys. Rev. B* **1976**, *13*, 5188-5192.

(5) (a) Fu, D.-W.; Cai, H.-L.; Liu, Y.; Ye, Q.; Zhang, W.; Zhang, Y.; Chen, X.-Y.; Giovannetti, G.; Capone, M.; Li, J.; Xiong, R.-G. Diisopropylammonium Bromide Is a High-Temperature Molecular Ferroelectric Crystal. *Science* **2013**, *339*, 425-428; (b) Fu, D.-W.; Zhang, W.; Cai, H.-L.; Ge, J.-Z.; Zhang, Y.; Xiong, R.-G. Diisopropylammonium Chloride: A Ferroelectric Organic Salt with a High Phase Transition Temperature and Practical Utilization Level of Spontaneous Polarization. *Adv. Mater.* **2011**, *23*, 5658-5662.

(6) Grimme, S.; Antony, J.; Ehrlich, S.; Krieg, H. A Consistent and Accurate *Ab Initio* Parametrization of Density Functional Dispersion Correction (DFT-D) for the 94 Elements H-Pu. *J. Chem. Phys.* **2010**, *132*, 154104.

(7) Sun, J.; Ruzsinszky, A.; Perdew, J. P. Strongly Constrained and Appropriately Normed Semilocal Density Functional. *Phys. Rev. Lett.* **2015**, *115*, 036402.

(8) Sabatini, R.; Gorni, T.; de Gironcoli, S. Nonlocal Van Der Waals Density Functional Made Simple and Efficient. *Phys. Rev. B* **2013**, *87*, 041108.

(9) Peng, H.; Yang, Z.-H.; Perdew, J. P.; Sun, J. Versatile van der Waals Density Functional Based on a Meta-Generalized Gradient Approximation. *Phys. Rev. X* **2016**, *6*, 041005.

(10) Allen, M. P.; Tildesley, D. J., *Computer Simulation of Liquids*. Revised ed.; Oxford University Press: New York, 1991.

(11) (a) Parrinello, M.; Rahman, A. Crystal Structure and Pair Potentials: A Molecular-Dynamics Study. *Phys. Rev. Lett.* **1980**, *45*, 1196-1199; (b) Parrinello, M.; Rahman, A. Polymorphic Transitions in Single Crystals: A New Molecular Dynamics Method. *J. Appl. Phys.* **1981**, *52*, 7182-7190.